Journal of Photochemistry & Photobiology A: Chemistry 388 (2020) 112158

Contents lists available at ScienceDirect

Journal of Photochemistry & Photobiology A: Chemistry

journal homepage: www.elsevier.com/locate/jphotochem

Cavity size dependent stoichiometry of probe–cyclodextrin complexation: Experimental and molecular docking demonstration

Sinjan Das[a], Surjatapa Nath[b], T. Sanjoy Singh[b], Nitin Chattopadhyay[a,*]

[a] Department of Chemistry, Jadavpur University, Jadavpur, Kolkata, 700032, India
[b] Department of Chemistry, Assam University, Silchar, Assam, 788011, India

ARTICLE INFO

Keywords:
Cyclodextrin
Benzonitrile based Schiff base
Inclusion complex
Stoichiometry
1:1 and 1:2 probe-CD complexation
Molecular docking

ABSTRACT

Host-guest interaction of a newly synthesized intramolecular charge transfer (ICT) probe, namely (E)-4-(4-(diethylamino)benzylideneamino)-2-(trifluoromethyl)benzonitrile (DBTFB), with supramolecular assemblies like α- and β-cyclodextrin (CD) has been investigated exploiting various spectroscopic techniques. Steady state fluorescence studies reveal that depending on the different cavity sizes of the hosts, probe–CD inclusion complexes of different stoichiometries are formed. The stoichiometries and association constants of these complexes have been determined exploiting Benesi-Hildebrand equation and the stoichiometries are found to be 1:1 and 1:2 for probe–α-CD and probe–β-CD inclusion complexes respectively. Relatively higher steady state fluorescence anisotropy value of the probe in β-CD compared to that in α-CD substantiates the stoichiometrically different probe–CD interactions. Time resolved fluorescence study further corroborates the differential stoichiometry in the two cases. Hydrodynamic diameters of CD-encapsulated probe as obtained from dynamic light scattering (DLS) experiments demonstrate the cyclodextrin dependent stoichiometries. Molecular docking has been exploited to get a qualitative molecular based picture of the probe–CD complexations in the two cases.

1. Introduction

Cyclodextrins (CDs) belong to an important class of supramolecules which are derived from the enzymatic transformation of the essential polysaccharide, starch [1]. Cyclodextrins are cyclic oligomers, consisting of α-D-glucose subunits joined by α-1,4 glycosidic bonds. Three popular and well known ones are α-, β- and γ-CD consisting of 6, 7 and 8 glucopyranose units respectively (Scheme 1(A)). CDs possess a cage-like supramolecular structure bearing similarity with cryptands, calixarenes, cyclophanes and spherands. They have truncated cone like shapes, with the larger and smaller openings of the cone exposed to the solvent through secondary and primary hydroxyl groups respectively [1]. Owing to this specific arrangement, the exterior part is sufficiently hydrophilic to impart solubility of CDs in water. On the contrary, the interior is considerably hydrophobic and they have an internal cavity accessible to the guest molecules of appropriate dimension through an opening of 4.5–5.3 Å, 6.0–7.0 Å and 7.5–8.5 Å for α-, β- and γ-CD respectively with more or less same cavity depth of 7.9 Å [2,3]. For host-guest interaction between CDs and the entrapped guest molecules no covalent bonding takes place. However, due to the action of weak noncovalent forces like hydrogen bonding, hydrophobic interactions, and van der Waals forces the guest molecules remain within the CD cavity, keeping the entire system in equilibrium with free host and guest molecules [2,3]. Through host-guest interaction with CDs, remarkable modification of different physicochemical and/or biological characteristics of the guest molecules can be achieved [1–3]. CDs have found wide applications encompassing diverse areas of synthetic, analytical, food, pharmaceutical chemistry, biotechnology, nanotechnology etc. [4]. Non-toxic nature [5,6] and water solubility of CDs make them suitable candidates for carriers in targeted drug delivery as well as drug excretion to remove excess drugs accumulated in the cell membranes [4,7,8]. Since their discovery, study of the structural modification and application oriented aspects of CDs are, therefore, considered as thriving arena of research to the global scientific community.

Extensive research has been carried out by many groups throughout the world for past few decades to divulge the intricacies behind different probe–CD interactions as well as to understand the mechanistic details of a number of photoprocesses like excited state proton transfer (ESPT), excited state intramolecular proton transfer (ESIPT), intramolecular charge transfer (ICT), and so forth [9–16]. Nonetheless, it is well established that depending on the dimension of the cavities, CDs are capable of encapsulating guest molecules of different dimensions with 1:1, 1:2, 2:1 and 2:2 type probe-CD stoichiometries [4,16–21].

* Corresponding author.
E-mail address: nitin.chattopadhyay@yahoo.com (N. Chattopadhyay).

https://doi.org/10.1016/j.jphotochem.2019.112158
Received 22 August 2019; Received in revised form 24 September 2019; Accepted 10 October 2019
Available online 18 October 2019
1010-6030/

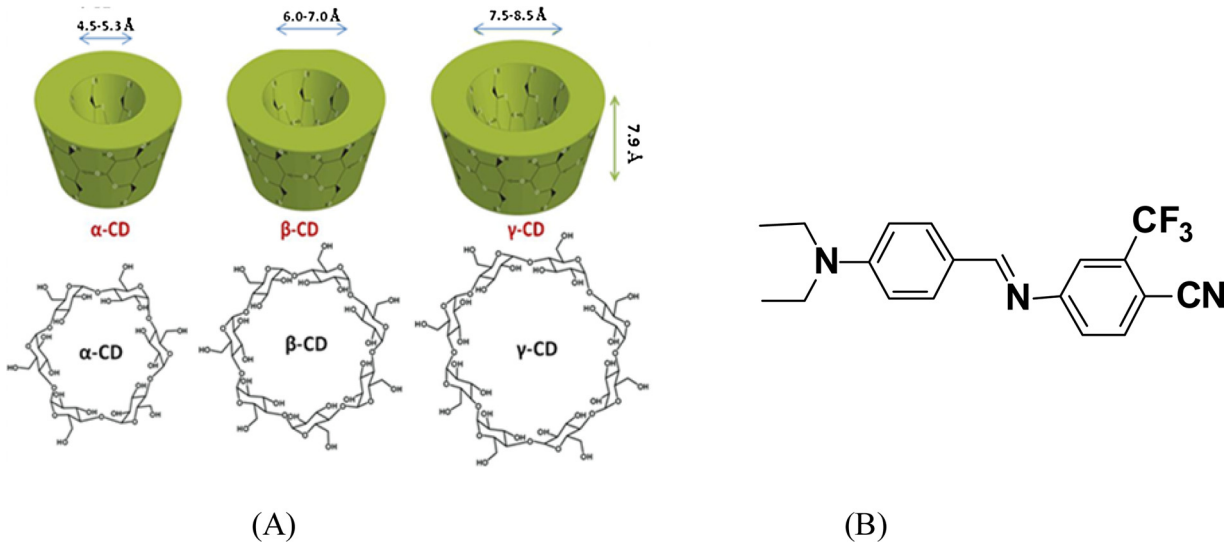

Scheme 1. (A) Schematic structures of α-, β- and γ-CD. (B) Chemical structure of DBTFB.

Formation of probe anchored extended nanotubes is also reported in this context [22]. Differential formation of such stochiometrically driven probe–CD complexes are of special interest from the viewpoint of the contemporary therapeutic research.

Schiff bases are one of the mostly studied organic compounds for various reasons. Apart from their use as dyes and pigments, precursors as well as intermediates in organic synthesis and catalysis, due to their antibacterial, antifungal, antimalarial, anti-inflammatory and antipyretic activities they have wide-spread applications in pharmaceutical industries as well [23,24]. The highly active imine group present in these Schiff base compounds is attributed responsible for their diverse bio-activity which can be tuned by proper substitution in the molecular framework of the compounds [24–26]. Selective metal binding affinity of the Schiff bases is exploited to fabricate different chemosensors [27–30]. Among the various classes of Schiff base compounds, benzonitrile based Schiff bases have acquired importance because of their application in fabricating photorefractive materials known for their potential use in optical processing [31]. Considering the importance of the benzonitrile based Schiff bases, a new Schiff base, namely (E)-4-(4-(diethylamino)benzylideneamino)-2-(trifluoromethyl) benzonitrile, abbreviated as DBTFB (Scheme 1(B)), containing diethylamino group as the donor at one end, and nitrile and trifluoromethyl groups as the acceptor groups at the other, is synthesized. The photophysical aspects of the compound, mainly the ICT behavior, have been studied exploiting different spectroscopic techniques. However, in the present work major emphasis has been given to investigate the host-guest interaction of the probe with α- and β-CDs. Since this is the first report of photophysics of the newly synthesized probe DBTFB, we have intended to report, in some depth, its host-guest interaction with CDs with an optimistic view that the probe might be effective in some application in future. Analyzing the steady state fluorometric data, it is found that DBTFB forms 1:1 and 1:2 inclusion complexes with α- and β-CD respectively, governed by the dimension of the CD cavities. Time resolved fluorescence decays of the probe in the studied microheterogeneous environments justify the observations from the steady state emission studies. Further, steady state fluorescence anisotropy, dynamic light scattering (DLS) study and molecular docking simulation have been exploited to validate cavity size dependent formation of different stoichiometries of the probe–CD complexes. The present work will help us to understand the intricacies of the differential behavior of benzonitrile based Schiff base molecular systems within varying dimensions of cyclodextrins. Hence, it will provide us valuable insight to find suitable drug formulation as well as drug delivery system, based on the requirement of the particular drug or the carrier to be used.

2. Experimental

2.1. Materials

4-(diethylamino)benzaldehyde and 4-amino-2-(trifluoromethyl) benzonitrile were procured from Sigma-Aldrich, USA, and were used without further purification for the synthesis of the fluorescent probe, DBTFB. α- and β-cyclodextrin and spectroscopic grade solvents such as methanol, acetonitrile and heptane were also obtained from Sigma-Aldrich, USA, and were used as received. AR grade acetic acid and nitric acid were obtained from Merck, India. To prepare a stock solution of DBTFB spectroscopic grade methanol was used and the final volume of methanol in the experimental solutions was kept below 2%. Deionized water from a Milli-Q purification system (Millipore) was used for the preparation of aqueous solutions to work with the CDs. Concentration of DBTFB was kept at ~ 4 μM throughout the experiment. All the experiments were performed at room temperature (27 °C) with air-equilibrated solutions.

2.2. Synthesis and characterization

(E)-4-(4-(diethylamino)benzylideneamino)-2-(trifluoromethyl)benzonitrile (DBTFB) was synthesized by one step condensation of 4-(diethylamino)benzaldehyde (0.177 g, 1 mmol) and 4-amino-2-(trifluoromethyl)benzonitrile (0.186 g, 1 mmol) under reflux condition for 3 h in the presence of 2–3 drops of acetic acid. Since the reaction led to precipitation of the product DBTFB, it was easy to follow the reaction. However, the progress of the reaction was checked by thin layer chromatography (TLC) taking the reaction mixture time-to-time using hexane/ethyl acetate mixture as eluent. The precipitate was filtered, washed with cold ethanol for three times and then recrystallized twice from warm ethanol to get dark yellow microcrystals of DBTFB in 80% yield and its purity was checked from TLC. The melting point (mp) of the compound was found to be 138 °C. The compound was characterized by FTIR, ^{1}H NMR, mass spectra and elemental analysis. The ^{1}H NMR and mass spectra are provided in Figs. S1 and S2 respectively. IR (ν_{max}, cm^{-1}, KBr): 3192 (ν_{as}(C−H)), 3047 (ν_s(C−H)), 2250 (ν(C≡N)), 1596 (ν(C═N)), 1572 (ν(C═C)), 1128 (ν(C−N)). ^{1}H NMR (500 MHz, $CDCl_3$, TMS, δ, ppm) δ: 1.2 (6H, t, 7 Hz), 3.6 (4H, m), 6.75 (1H, d, 8.5 Hz), 6.93 (1H, s), 7.2 (1H, d, 8 Hz), 7.54 (1H, d, 8.5 Hz), 7.83 (1H, d, 8 Hz), 7.98 (2H, d, 7.5 Hz) and 9.98 (1H, s). TOF-MS-ES+: for

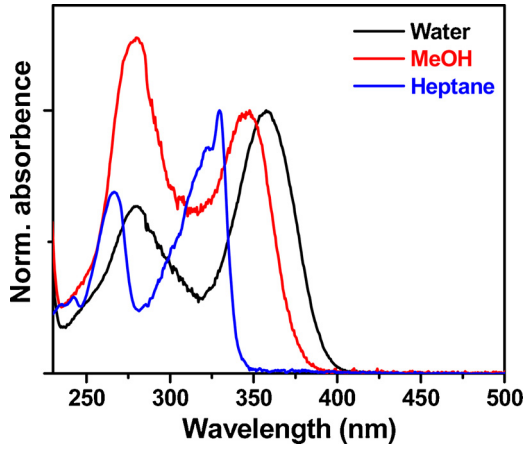

Fig. 1. Normalized absorption spectra of DBTFB in different solvents as mentioned in the legend.

$C_{19}H_{18}F_3N_3$ $[M^+ + H]^+$: 346.06. Anal. Calc. for $C_{19}H_{18}F_3N_3$ (345.15): C, 66.08%; H, 5.21%; N, 12.17%. Found: C, 66.05%; H, 5.25%; N, 12.69%.

2.3. Methods

A Perkin Elmer L120-00A spectrometer was employed for the IR analysis of the sample using KBr pellets in the range of 4000-400 cm^{-1}. A Bruker (500 MHz) instrument was used for proton NMR and the chemical shifts were relative to tetramethylsilane. ESI mass spectrum was recorded on a Waters XEVO G2 QTof mass spectrometer. The elemental analysis was carried out on a Perkin Elmer PE2400 elemental analyzer. Absorption studies were carried out on a Shimadzu UV-2450 spectrophotometer (Shimadzu Corporation, Japan). For steady state fluorescence and fluorescence anisotropy measurements a Horiba Jobin Yvon Fluoromax-4 spectrofluorometer was employed. Fluorescence anisotropy (r) is defined as [32],

$$r = (I_{VV} - G \cdot I_{VH}) / (I_{VV} + 2\,G \cdot I_{VH}) \quad (1)$$

where I_{VV} and I_{VH} are the emission intensities obtained with the excitation and emission polarizers set at (0°, 0°) and (0°, 90°), respectively. G, an instrument factor, is given by [32],

$$G = I_{HV}/I_{HH} \quad (2)$$

where I_{HV} and I_{HH} correspond to the emission signals for excitation and emission polarizers set at (90°, 0°) and (90°, 90°), respectively.

Fluorescence lifetime measurements were performed using time correlated single photon counting (TCSPC) principle on an Edinburgh Instrument using a nanosecond diode laser at 295 nm (IBH, UK) as the light source. The decays were analyzed using IBH DAS-6 decay analysis software. The acceptability of the fitted data was appraised from the χ^2 criterion (within 1–1.2) and inspection of the residuals of the data to the fitted function. Mean fluorescence lifetimes (τ_{avg}) for bi-exponential iterative fittings were calculated from the decay times (τ_i) and the pre-exponential factors (a_i) using the following relation:

$$\tau_{avg} = a_1\tau_1 + a_2\tau_2 \quad (3)$$

Dynamic light scattering (DLS) measurements were carried out on a Malvern Nano-ZS90 instrument equipped with a He-Ne laser (λ = 632.8 nm). The operating procedure is programmed with a DTS software. Samples were filtered with 0.1 μm syringe filter (Merck Millipore Ltd.) prior to the measurements. For each measurement, mean was taken over 15 runs and each run was averaged for 20 s.

Quantum chemical calculations were performed using Gaussian 09 software [33] to obtain energy minimized structure of DBTFB. The ground state calculations were carried at density functional theory (DFT) using CAM-B3LYP [34–38] as the exchange correlation functional and 6-311 + + G** basis set. The geometry optimizations of DBTFB in different solvents were performed at the same level with DFT based conductor polarizable continuum model (CPCM) [39,40]. The UV–vis absorption spectra of the probe in water and heptane were simulated from the vertical transitions of the ground state optimized geometry at the TDDFT/CAM-B3LYP/6-311 + + G** level with CPCM model using appropriate solvents. Electronic distribution of the probe at the highest occupied molecular orbital (HOMO) and lowest unoccupied molecular orbital (LUMO) were obtained from the ground state optimized geometry of DBTFB.

The AutoDock-vina program (version 1.1.2) [41], providing better accuracy than the Autodock 4 software [41–43] in predicting the mode of binding, was exploited for the molecular docking simulations. For the docking study, the output file of the ground state optimized geometry of DBTFB as obtained from the procedure stated above was converted into a compatible protein data bank (pdb) file. We have adopted the tangible and widely accepted crystal structures of α- and β- cyclodextrins [44–46] and hence their corresponding pdb files [47] in our docking study. Prior to the simulation, MGLTools (version 1.5.6) was used to convert the receptor and ligand coordinate files into PDBQT format. A three dimensional grid box of dimension 70 × 70 × 70 was constructed with a grid spacing of 0.375 Å. The grid box was created in such a fashion that it would be large enough to include not only the respective CD cavities but also the whole encapsulated structures. For docking simulation, 20 different conformations were taken into account to find out the lowest energy docked conformer. The PyMOL software package was used for visualization of the docked poses and analyzing the corresponding conformations [48].

3. Result and discussion

3.1. Steady state absorption study

Room temperature absorption spectra of DBTFB in different solvents are shown in Fig. 1. In all the studied solvents absorption spectra of DBTFB are found to be grossly of similar pattern. The spectrum exhibit two bands, one around 250–300 nm and the other around 300–400 nm. The low energy absorption band shows a significant bathochromic shift (~ 30 nm) of the band maximum with increase in the polarity of the solvents from heptane to water (Fig. 1). On the other hand, a smaller bathochromic shift (~ 12 nm) of the band maximum for the high energy band is observed with increase in the polarity of the studied solvents. The low sensitivity of higher energy band towards the solvent polarity implies that the band originates due to the π–π* transition of the probe, whereas the significant solvatochromic response of the lower energy band indicates the band to have a charge transfer character.

To check whether the lower energy absorption band of DBTFB is a charge transfer (CT) band or not, the effect of addition of acid (dilute nitric acid) on this band has been studied. Gradual addition of acid to the methanolic solution of DBTFB leads to a considerable decrease in the intensity of the lower energy absorption band (Fig. S3). The observation can be rationalized by considering the fact that upon addition of the acid, the lone pair of electrons on nitrogen of the diethylamino moiety is consumed while protonation takes place and thereby the transfer of electron density from the donor diethylamino end to the nitrile and trifluoromethyl end of DBTFB is restricted. This indicates that charge transfer takes place in the ground state and the corresponding absorption band of DBTFB is a CT band. Molecular orbital diagram of DBTFB (Fig. 2) obtained from DFT based HOMO-LUMO calculation also reveals the charge transfer process from the diethylamino part to the other end of the probe. In HOMO we can see that the electron density is mainly localized over the diethylamino part and its associated benzene ring; whereas in LUMO it is observed that the electron density over the nitrile and its associated benzene ring of the molecule is increased remarkably at the cost of the decreased electron

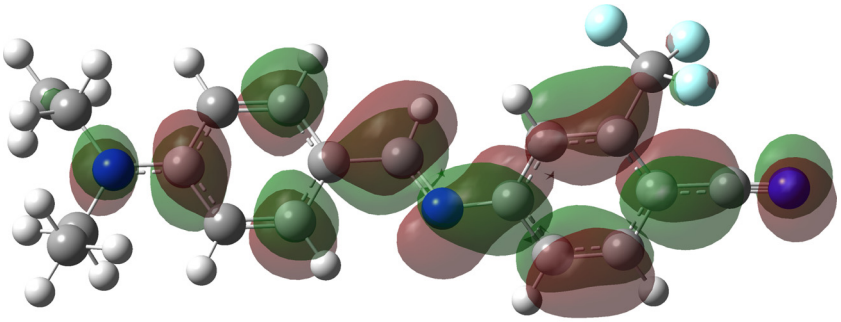

LUMO

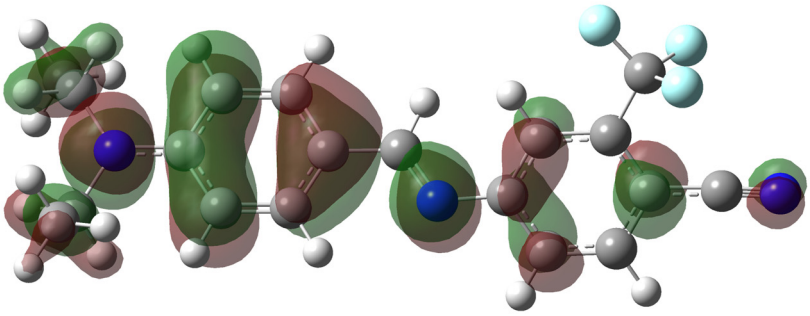

HOMO

Fig. 2. Molecular orbital (MO) pictures (HOMO and LUMO) of DBTFB.

density over diethylamino end, justifying the charge transfer from the diethylamino end to the nitrile end of the fluorophore.

An endeavor is also made to reproduce the absorption spectra of DBTFB in the said solvents through simulation. To obtain the simulated absorption spectra of the fluorophore in heptane and water, vertical transitions were calculated taking the ground state optimized geometries of the fluorophore using TDDFT method with CAM-B3LYP/6-311 + +G** basis set with CPCM model. The pattern of the simulated spectra go parallel to the experimental ones and the band maxima agree reasonably well with those of the experimentally obtained ones in the respective solvents (Table S1) establishing the reliability of the simulation procedure.

Now, to study the effect of α- and β-CD on the absorption spectrum of DBTFB, the CDs were gradually added ([α-CD] = 0–20 mM and [β-CD] = 0–9 mM) to the aqueous solution of DBTFB (Fig. S4). However, No appreciable change was observed in the absorption spectra of the probe with the gradual addition of either of the two CDs. Absorption technique being less sensitive than emission, we have given emphasis on the fluorometric study.

3.2. Steady state emission study

Upon photoexcitation at the CT band of DBTFB, no emission has been observed. However, changing the excitation wavelength to 280 nm, i.e., at π–π* band, reveals a broad unstructured emission band with emission maximum in the range ~ 340–400 nm depending on the polarity of the solvents (Fig. 3). This anomalous behavior of the emission spectrum of DBTFB might be rationalized by the relative distributions and corresponding energy gaps between the excited singlet and triplet states of DBTFB and appears to be an interesting topic for further spectroscopic research [49]. However, polarity sensitivity of the emission band of the probe upon excitation at the π–π* absorption band is quite interesting. The bathochromic shift of the emission maximum of

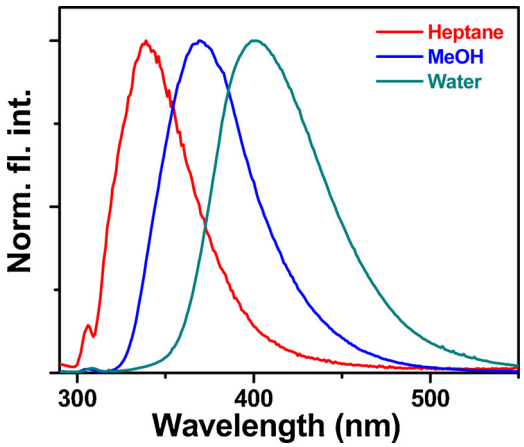

Fig. 3. Normalized emission spectra of DBTFB in different solvents as depicted in the legend. λ_{ex} = 280 nm.

the probe with increasing solvent polarity (Fig. 3) implies that charge transfer takes place in the excited state as well. In the present work, not going into the detailed intricacy of the photophysical aspects of DBTFB, we focus our interest in divulging the effect of CDs on the emission behavior of the probe in aqueous medium.

To avoid any interference from the absorption of the added cyclodextrins absorbing in the range 260–300 nm and to excite DBTFB preferably at its CT band, in the present case the optimum excitation wavelength is chosen as 330 nm throughout the steady state study. On excitation at 330 nm, emission spectrum of aqueous solution of DBTFB gives the same broad and unstructured band with maximum at around 400 nm (black spectrum in Fig. 4) similar to that obtained with 280 nm excitation. Gradual addition of α- or β-CDs leads to significant enhancements in the fluorescence intensity of the probe compared to that

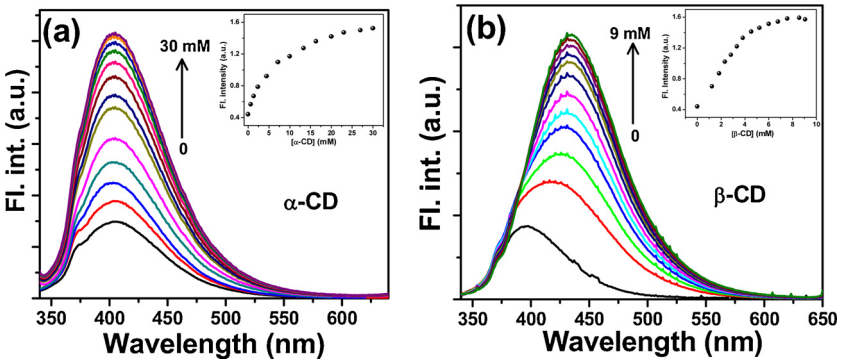

Fig. 4. Emission spectra (λ_{ex} = 330 nm) of DBTFB with the gradual addition of (a) α-CD and (b) β-CD.

in pure aqueous medium as depicted in Fig. 4. Considerable change in the emission intensities of the probe in the CD environments indicates that there is substantial interaction between the probe and the CDs referring to the formation of probe–CD inclusion complexes. The enhancement in the fluorescence intensity can be justified by a reduction in the non-radiative decay rate, possibly because of enhanced rigidity in the immediate environment of the probe compared to that in bulk aqueous medium [11–17,32]. It is pertinent to mention here that no appreciable change in the emission maximum is observed in case of probe–α-CD interaction (Fig. 4(a)). On the contrary, a large bathochromic shift of ~ 35 nm is observed for probe–β-CD complexation (Fig. 4(b)). This large red shift suggests that the probe experiences higher polarity in its vicinity as evidenced from the polarity dependent red shift in the emission maximum of the probe in pure solvents. The plausible reason behind this shift might be due to the positioning of the polarity sensitive parts of DBTFB at the rim regions of β-CD where the probe effectively experiences higher polarity caused by the high density of hydroxyl groups of β-CD in the vicinity of its polar groups due to the encapsulation. Chattopadhyay et al. had categorically established that the proton from CD encapsulated carbazole molecule could be extracted by external base through a cooperative proton transfer *via* the rim hydroxyl groups of the CDs using bidirectional flip-flop hydrogen bonding, justifying the pivotal role of the hydroxyl groups in the rim region of β-CD in enhancing the local polarity around the probe [12,13]. A pictorial perceptualization can also be acquired from molecular docking simulation (see later) as an evidence for the relative position of the polar parts of the probe in the β-CD environment.

From this differential change in the emission maxima of the probe in α- and β-CD environments, it can be inferred that the probe interacts with the CDs in different ways and this is probably due to different types of host-guest complexation in different CD environments governed by their respective cavity sizes.

In order to determine the stoichiometries and the binding constants of the inclusion complexes, the dependence of the fluorescence intensity of DBTFB on the concentrations of different CDs were analyzed using Benesi-Hildebrand equations for 1:1 and 1:2 complexes (Eqs. (4) and (5) respectively) [50].

$$\frac{1}{\Delta F} = \frac{1}{\Delta F_{max}} + \frac{1}{K\Delta F_{max}} = \frac{1}{CD} \quad (4)$$

$$\frac{1}{\Delta F} = \frac{1}{\Delta F_{max}} + \frac{1}{K\Delta F_{max}} = \frac{1}{[CD]^2} \quad (5)$$

where $\Delta F = F_x - F_0$ and $\Delta F_{max} = F_\infty - F_0$, with F_0, F_x and F_∞ being the fluorescence intensities of the free probe molecule, at an intermediate CD concentration and at the end of probe-CD complex formation respectively. In case of probe–α-CD complex, the plot of 1/ΔF against 1/[CD] shows linearity over the entire concentration range of α-CD, justifying 1:1 complexation according to Eq. (1) (Fig. 5(a)). However, when the same 1/ΔF is plotted against $1/[CD]^2$ to check whether, in any case, it may show the signature of 1:2 complexation, it is revealed that the plot clearly deviates from linearity (Fig. 5(b)) ruling out the possibility of 1:2 guest-host interaction. On the contrary, for β-CD, the plot of 1/ΔF against 1/[CD] shows a clear deviation from linearity (Fig. 6(a)) indicating that the complexation between the probe and β-CD is not of 1:1 stoichiometry. However, when 1/ΔF is plotted against $1/[CD]^2$ it obeys Eq. (5) and fits to linearity over the entire range of β-cyclodextrin concentration as depicted in Fig. 6(b) implying formation of 1:2 probe − β-CD complex. Once the stoichiometries are known, the equilibrium binding constants of complex formation processes are determined from the individual linear double reciprocal plots. The calculated values are determined to be 1.59×10^2 L mol^{-1} for 1:1 probe–α-CD binding and 1.47×10^5 L^2 mol^{-2} for 1:2 binding in case of β-CD respectively, revealing that the nature of binding interaction of the probe with the two CDs are very different.

3.3. Steady state fluorescence anisotropy study

Fluorescence anisotropy, a fundamental photophysical parameter, dictates the motional restriction imposed on the fluorophore by the immediate environment and hence, often serves as a tool for exploring the location of the fluorophore in bio- and biomimetic microheterogeneous environments like protein, lipid, DNA, micelle, cyclodextrin, etc. [6,21,22,32,51–54]. In most of the low viscous solvents, the photoexcited fluorophore rotates very fast within its fluorescence lifetime, revealing very low (close to zero) values of fluorescence anisotropy [32]. However, increase in the viscosity of the medium or enhanced effective volume of the probe due to some specific interaction among the probe molecules or between the probe and the solvent, might restrict the rotation process of the probe leading to an increase in its fluorescence anisotropy [32,55,56].

In the present case, DBTFB reveals very low fluorescence anisotropy value in aqueous medium which indicates that the probe rotates freely in aqueous medium without any rotational restriction. With the gradual addition of α- and β-CDs, the fluorescence anisotropy value of the probe gradually increases and reaches the respective plateaus (Fig. 7). From Fig. 7, it is evident that fluorescence anisotropy value of the probe in β-CD is much higher compared to that in α-CD. It is known that the effective dimension of a fluorophore puts its signature on the rotational motion of the fluorophore; bigger one restricting the rotation of the fluorophore more, resulting in a higher fluorescence anisotropy. Hence, the higher anisotropy value of DBTFB in β-CD solution compared to that in α-CD indicates that the effective size of the probe–β-CD complex is remarkably bigger than the complex of the probe with α-CD (see later). Hence, the rotational motion of the probe–β-CD inclusion complex is retarded to a greater extent compared to the inclusion complex with α-CD, resulting in a higher anisotropy value in the former case. Thus, the appreciable difference in the saturation fluorescence anisotropy values of the probe in α- and β-CD, as evident from Fig. 7, implies that the binding interactions of the probe with two CDs are not of similar type and corroborate 1:1 probe-CD binding with α-CD and 1:2 binding with

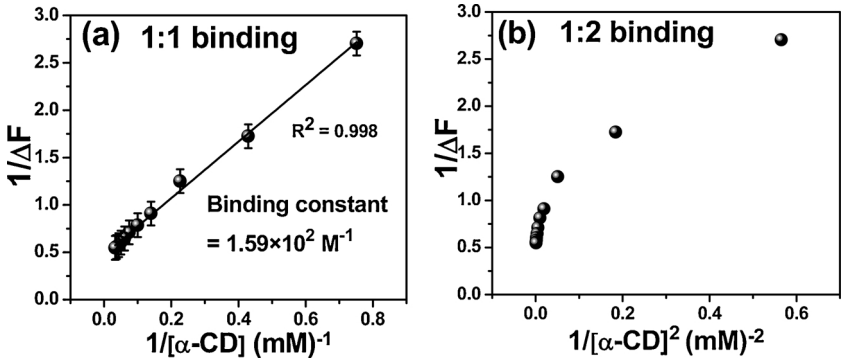

Fig. 5. Double reciprocal plots for complexation between DBTFB and α-CD in aqueous solution. Plots of (a) $1/\Delta F$ vs. $[\alpha\text{-CD}]^{-1}$ and (b) $1/\Delta F$ vs. $[\alpha\text{-CD}]^{-2}$.

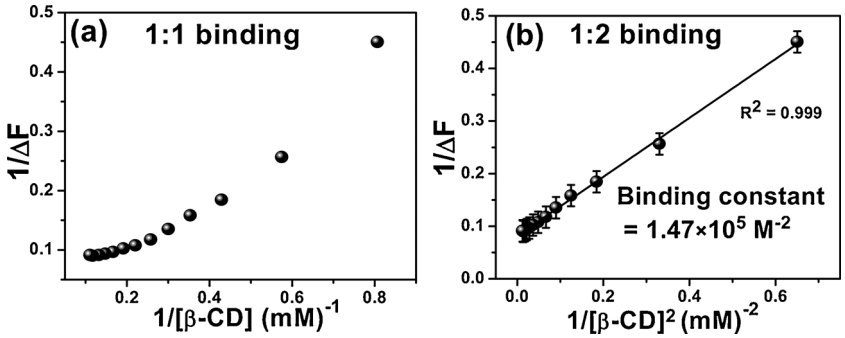

Fig. 6. Double reciprocal plots for complexation between DBTFB and β-CD in aqueous solution. Plots of (a) $1/\Delta F$ vs. $[\beta\text{-CD}]^{-1}$ and (b) $1/\Delta F$ vs. $[\beta\text{-CD}]^{-2}$.

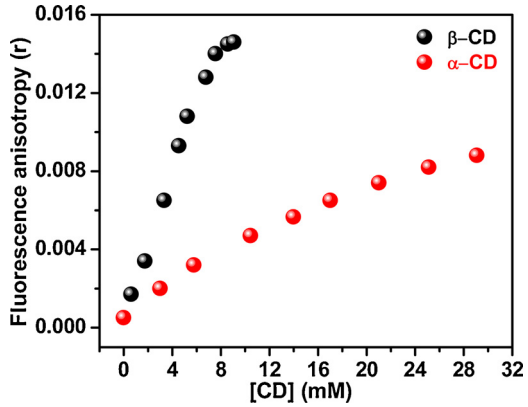

Fig. 7. Plot of variation of fluorescence anisotropy of DBTFB as a function of concentrations of CDs. Each anisotropy value is an average of 15 individual and consistent measurements. λ_{ex} = 330 nm and $\lambda_{moni} = \lambda_{em}^{max}$.

β-CD.

3.4. Time resolved fluorescence decay study

Since fluorescence lifetime study deals with the excited state phenomena of a fluorophore it is considered as a highly sensitive tool, and often used to extract valuable information regarding the location of the probe in various bio- and biomimicking environments, thereby providing information about the binding phenomenon [32,57]. Fluorescence intensity decay profiles of DBTFB in different environments are portrayed in Fig. 8 and the corresponding decay parameters are listed in Table 1. It is observed that the fluorescence decay of DBTFB in aqueous medium is single exponential in nature and in the presence of α- and β-CDs the decays become biexponential clearly giving an additional longer lifetime component. The change of pattern of fluorescence lifetime decays of DBTFB from mono-exponential to biexponential reflects the presence of the probe in two states: free and CD-bound. The enhancement in the fluorescence lifetime of DBTFB in the presence of CDs is ascribed to the formation of probe–CD inclusion complexes.

Fluorescence lifetime of DBTFB in water is found to be 1.35 ± 0.4 ns (Table 1). With the addition of α-CD, the shorter component (~ 1.4 ns) of the biexponential decay agrees with the decay of the probe in pure aqueous medium and it remains more or less constant over the entire concentration range of α-CD indicating the existence of the free probe in the medium (Fig. 8(a) and Table 1). On the other hand, the longer component shows an enhancement from 5.7 ns to 8.7 ns with the addition of α-CD, referring to the formation of probe–α-CD complex, consistent with the steady state emission study. The variation in the contributions of the lifetime components is found to be nominal in case of probe–α-CD complex (Fig. S5(a)). However, a slight increment is observed in the average lifetime of the probe (from ~ 1.4 ns to ~ 1.7 ns) in the presence of α-CD (Table 1) compared to that in pure aqueous medium.

In case of β-CD, both the shorter and longer components increase with the gradual addition of β-CD as shown in Fig. 8(b) and Table 1. Though in both α- and β-CD the lifetime decays are biexponential in nature, the pattern in the presence of β-CD is visibly different from the same in the presence of α-CD. The shorter component increases from ~ 1.4 ns to ~ 1.9 ns whereas the longer component shows an enhancement from ~ 8 ns to ~ 12 ns. Moreover, the variation in the respective contributions of the lifetime components is more prominent in case of probe–β-CD complexation (Fig. S5(b)). The average fluorescence lifetime of DBTFB in β-CD medium shows a significant increase relative to that in water (from ~ 1.4 ns to ~ 4.5 ns). The significant difference in the relative contributions of the lifetime components of DBTFB in the presence of α- and β-CD also implies formation of different types of probe–CD inclusion complexes in the two situations. Therefore, with gradual addition of both the CDs the probe interacts with them differently and it experiences different microenvironments around it in these two media which goes in favor of 1:1 and 1:2 stoichiometries between the probe and α- and β-CDs respectively.

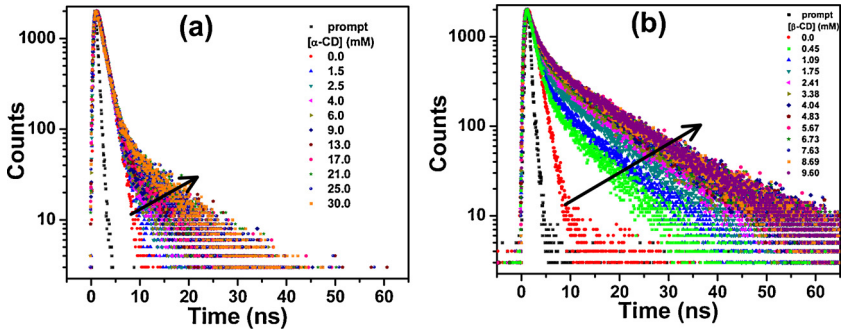

Fig. 8. Fluorescence decay profiles of DBTFB in (a) α- and (b) β-CD. The legends of the figures contain the concentrations of CDs. λ_{ex} = 295 nm, λ_{moni} = 400 nm and 430 nm for α- and β-CD respectively.

Table 1
Fluorescence lifetime data of DBTFB in different environments.

Environment	[CD] (mM)	$\tau_1 \pm 0.4$ (ns)	$\tau_2 \pm 0.4$ (ns)	a_1	a_2	$\tau_{avg} \pm 0.4$ (ns)	χ^2
Water		1.35	–	1.00	–	1.35	1.02
α-CD	1	1.34	5.68	0.99	0.01	1.38	1.07
	1.5	1.36	6.74	0.98	0.02	1.47	1.01
	2.5	1.36	6.91	0.98	0.02	1.47	1.01
	4.0	1.38	7.45	0.98	0.02	1.50	1.02
	6.0	1.40	7.85	0.98	0.02	1.53	1.11
	9.0	1.42	8.69	0.97	0.03	1.64	1.00
	13.0	1.41	8.68	0.96	0.04	1.70	1.25
	17.0	1.41	8.52	0.96	0.04	1.69	1.01
	21.0	1.41	8.54	0.96	0.04	1.70	1.00
	25.0	1.42	8.57	0.96	0.04	1.71	1.17
	30.0	1.42	8.72	0.96	0.04	1.71	1.03
β-CD	0.45	1.34	8.09	0.91	0.09	1.95	1.10
	1.09	1.50	9.15	0.89	0.11	2.34	1.00
	1.75	1.61	10.48	0.84	0.16	3.03	1.14
	2.41	1.66	11.06	0.78	0.22	3.73	1.07
	3.38	1.73	11.49	0.77	0.23	3.97	1.15
	4.04	1.74	11.67	0.74	0.26	4.32	1.11
	4.83	1.76	11.75	0.74	0.26	4.36	1.06
	5.67	1.79	11.97	0.74	0.26	4.44	1.11
	6.73	1.82	12.00	0.74	0.26	4.47	1.16
	7.63	1.83	12.06	0.74	0.26	4.49	1.03
	8.69	1.81	11.98	0.74	0.26	4.45	1.11
	9.60	1.88	11.91	0.74	0.26	4.49	1.00

3.5. Dynamic light scattering study

To throw light, particularly on the size aspect of the probe–CD complexes and hence to divulge the stoichiometry, the dynamic light scattering (DLS) technique has been adopted. Since the dimension of the free probe molecule falls within the instrumental resolution limit of our set-up (1.0 nm), no size distribution is observed for it in aqueous medium. Smaller size of the probe molecule in aqueous medium also gets support from its very low fluorescence anisotropy. To divulge the effect of α-CD and β-CD on the probe, the size distributions of α- and β-CD are measured in the absence and presence of the probe and are depicted in Fig. 9 (raw data is presented in Fig. S6). The corresponding hydrodynamic diameters are listed in Table 2. The diameters of α- and β-CD without the probe are found to be 1.2 nm and 1.5 nm agreeing well with the literature reports [58,59]. In the presence of the probe, slight enhancement is observed in the hydrodynamic diameter of α-CD (from 1.2 nm to 1.37 nm) relative to that in the absence of the probe corroborating 1:1 binding interaction between the probe and α-CD. On the contrary, the dimension of the DBTFB–β-CD complex becomes more than double the dimension of β-CD in the absence of probe, which clearly points to the formation of 1:2 probe–β-CD complex justifying the steady state and time resolved observations.

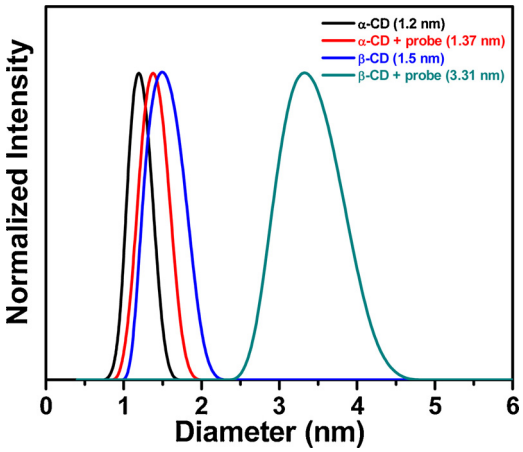

Fig. 9. Normalized size distributions of α- and β-CD in the presence and absence of DBTFB.

Table 2
Hydrodynamic diameters of CDs in the absence and presence of DBTFB.

Species	Hydrodynamic diameter (nm) (± 0.2)
α-CD	1.20
α-CD + DBTFB	1.37
β-CD	1.50
β-CD + DBTFB	3.31

3.6. Molecular docking study

Molecular docking simulation study has been employed to give qualitative support to our proposition of cavity size dependent stoichiometry of DBTFB–CD complexation as well as to visualize the mode of interaction between the probe and the CDs. For 1:1 stoichiometry, the CD monomer is chosen as the "receptor" and DBTFB as the "ligand". The binding energy of the lowest energy docked conformer of DBTFB–α-CD inclusion complex with 1:1 stoichiometry (Fig. 10(a)) is found to be – 4.1 kcal mol^{-1}. On the other hand, DBTFB–β-CD complex with 1:1 stoichiometry reveals the binding energy to be – 4.8 kcal mol^{-1}. As the steady state and time resolved studies establish that the interaction between the probe and β-CD is different from that between the probe and α-CD, 1:2 probe–β-CD complexation has also been explored through docking simulation with obvious logic that the dimension of the cavity of β-CD is higher than that of α-CD. To overcome three molecule docking problem in 1:2 probe–β-CD complexation, following the steps of Nag et al. [46], two monomers of β-CD were arranged in head to head (HH) orientation and the separation between them was varied from 2 Å to 5 Å. It is pertinent to mention here that a gross approximation was accepted for this approach where the two β-

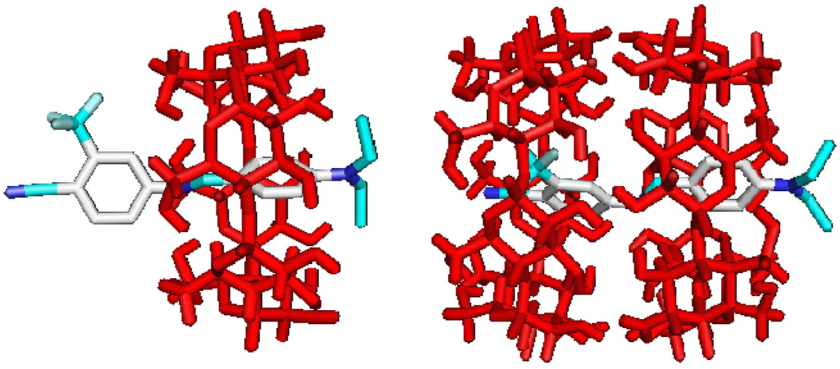

(a) (b)

Fig. 10. Lowest energy docked conformers of DBTFB within (a) α- and (b) β-CD cavity portraying 1:1 and 1:2 stoichiometry respectively.

CDs were not optimized in conjugated condition. Now, this coupled β-CD was treated as the “receptor” and DBTFB molecule as the “ligand”. The lowest energy conformer of DBTFB–β-CD complex shows 1:2 guest–host interaction where the separation between the two β-CD units remains ~ 2.5 Å (Fig. 10(b)) and the binding energy of the docked conformer is – 7.8 kcal mol^{-1} implying that the 1:2 probe–β-CD complex is more stabilized by about 3 kcal mol^{-1} than their 1:1 stoichiometry. Therefore, molecular docking simulation also demonstrates that the interaction of DBTFB with the two CDs is of different type and, thus, provides a pictorial support in favor of 1:1 and 1:2 probe–CD stoichiometries for complexation of the probe with α- and β-CDs respectively.

From Fig. 10(b), it can also be assessed that in 1:2 probe–β-CD inclusion complex the polar parts of the probe are situated at the rim regions of β-CD. As a result, the polar parts experience high density of hydroxyl groups of CDs in its vicinity enhancing the local polarity leading to the large bathochromic shift in the emission maximum of the probe in β-CD medium as discussed in Section 3.2.

4. Conclusion

The present work reports the study on the cavity size dependent stoichiometries of (E)-4-(4-(diethylamino)benzylideneamino)-2-(trifluoromethyl)benzonitrile (DBTFB), a newly synthesized benzonitrile based Schiff base compound containing "donor-acceptor" systems, with α- and β-CD exploiting different steady state and time resolved spectroscopic techniques. The results reveal that the photophysical behavior of DBTFB changes significantly upon encapsulation of the probe in the CD cavities. The variation of the emission properties with the addition of the CDs establishes that 1:1 and 1:2 probe–CD inclusion complexes are formed with α- and β-CD respectively. The differential changes of the fluorescence lifetime and the fluorescence anisotropy of the probe in the studied CD environments also imply that the probe experiences different microenvironments in these two media corroborating different stoichiometries for the host-guest inclusion complexation. The large enhancement in the hydrodynamic diameter of the probe–β-CD complex compared to that with the other cyclodextrin goes in favor of formation of 1:2 and 1:1 inclusion complexes respectively. Molecular docking study pictorially presents and endorses that the stoichiometries of DBTFB–CD inclusion complexes are different for the two cyclodextrins. The present work will be beneficial to understand the differential behavior of benzonitrile based Schiff base molecular systems within varying dimensions of supramolecular cyclodextrins, which might be useful in drug formulation as well as drug delivery.

Declaration of Competing Interest

The authors declare no conflict of interest.

Acknowledgements

Financial support from the Department of Science and Technology (grant numberEMR/2016/001087), Govt. of India, is gratefully acknowledged. The authors are thankful to Prof. Subhash Chandra Bhattacharya of the same department for DLS measurement. S.D. thanks University Grants Commission, New Delhi for his Senior Research Fellowship.

Appendix A. Supplementary data

Supplementary material related to this article can be found, in the online version, at doi:https://doi.org/10.1016/j.jphotochem.2019.112158.

References

[1] P. Caliceti, S. Salmaso, A. Semenzato, T. Carofiglio, R. Fornasier, M. Fermeglia, M. Ferrone, S. Pricl, Synthesis and physicochemical characterization of folate-cyclodextrin bioconjugate for active drug delivery, Bioconjugate Chem. 14 (2003) 899–908.
[2] S. Li, W.C. Purdy, Cyclodextrins and their applications in analytical chemistry, Chem. Rev. 92 (1992) 1457–1470.
[3] V.T. D’Souza, M.L. Bender, Miniature organic models of enzymes, Acc. Chem. Res. 20 (1987) 146–152.
[4] E.M. Martin Del Valle, Cyclodextrins and their uses: a review, Process Biochem. 39 (2004) 1033–1046.
[5] M.L. Bender, M. Komiyama, Cyclodextrin Chemistry, Springer – Verlag, Berlin, Germany, 1978.
[6] S. Ghosh, B.K. Paul, N. Chattopadhyay, Interaction of cyclodextrins with human and bovine serum albumins: a combined spectroscopic and computational investigation, J. Chem. Sci. 126 (2014) 931–944.
[7] T. Loftsson, P. Jarho, M. Másson, T. Järvinen, Cyclodextrins in drug delivery system, Expert Opin. Drug Deliv. 2 (2005) 335–351.
[8] P. Kundu, S. Das, N. Chattopadhyay, Managing efficacy and toxicity of drugs: targeted delivery and excretion, Int. J. Pharm. 565 (2019) 378–390.
[9] F. Cramer, W. Saenger, H.Ch. Spats, Inclusion compounds. XIX.[1a]The formation of inclusion compounds of α-cyclodextrin in aqueous solutions. Thermodynamics and kinetics, J. Am. Chem. Soc. 89 (1967) 14–20.
[10] K.A. Connors, The stability of cyclodextrin complexes in solution, J. Am. Chem. Soc. 97 (1997) 1325–1358.
[11] A. Nag, R. Dutta, N. Chattopadhyay, K. Bhattacharyya, Effect of cyclodextrine cavity size on twisted intramolecular charge transfer emission: dimethylamino benzonitrile in β-cyclodextrine, Chem. Phys. Lett. 157 (1989) 83–86.
[12] N. Chattopadhyay, Effect of cyclodextrin complexation on excited state proton transfer reactions, J. Photochem. Photobiol. A: Chem. 58 (1991) 31–36.
[13] N. Chattopadhyay, T. Chakraborty, A. Nag, M. Chowdhury, Effect of inclusion of cyclodextrin on excited state proton transfer: carbazole – γ-cyclodextrin, J. Photochem. Photobiol. A: Chem. 52 (1990) 199–204.
[14] S. Kundu, N. Chattopadhyay, Dual luminescence of dimethylaminobenzaldehyde in aqueous β-cyclodextrin: non-polar and TICT emissions, J. Photochem. Photobiol. A

88 (1995) 105–108.
[15] A. Banerjee, P.K. Sengupta, Encapsulation of 3-hydroxyflavone and fisetin in β-cyclodextrins: excited state proton transfer fluorescence and molecular mechanics studies, Chem. Phys. Lett. 424 (2006) 379–386.
[16] P. Hazra, D. Chakrabarty, A. Chakraborty, N. Sarkar, Intramolecular charge transfer and solvation dynamics of nile red in the nanocavity of cyclodextrins, Chem. Phys. Lett. 388 (2004) 150–157.
[17] A. Mallick, B. Haldar, N. Chattopadhyay, Encapsulation of norharmane in cyclodextrin: formation of 1:1 and 1:2 inclusion complexes, J. Photochem. Photobiol. B 78 (2005) 215–221.
[18] M.K. Singh, H. Pal, A.S.R. Koti, A.V. Sapre, Photophysical properties and rotational relaxation dynamics of neutral red bound to β-cyclodextrin, J. Phys. Chem. A 108 (2004) 1465–1474.
[19] S. Hamai, Inclusion of 2-chloronaphthalene by α-cyclodextrin and room-temperature phosphorescence of 2-chloronaphthalene in aqueous D-glucose solutions containing α-cyclodextrin, J. Phys. Chem. B 101 (1997) 1707–1712.
[20] D.W. Cho, Y.H. Kim, S.G. Kang, M. Yoon, D. Kim, Cyclodextrin effects on excited-state geometry change and intramolecular charge transfer of 4-biphenylcarboxylic acid, J. Phys. Chem. 98 (1994) 558–562.
[21] P. Das, A. Chakrabarty, B. Haldar, A. Mallick, N. Chattopadhyay, Effect of cyclodextrin nanocavity confinement on the photophysics of a β-carboline analogue: a spectroscopic study, J. Phys. Chem. B 111 (2007) 7401–7408.
[22] P. Das, A. Mallick, D. Sarkar, N. Chattopadhyay, Probe-induced self-aggregation of γ-cyclodextrin: formation of extended nanotubular suprastructure, J. Phys. Chem. C 112 (2008) 9600–9603.
[23] A. Kathiravan, K. Sundaravel, M. Jaccob, G. Dhinagaran, A. Rameshkumar, D. Arul Anath, T. Sivasudha, Pyrene schiff base: photophysics, aggregation induced emission, and antimicrobial properties, J. Phys. Chem. B 118 (2014) 13573–13581.
[24] Z. Guo, R. Xing, S. Liu, Z. Zhong, X. Li, L. Wang, P. Li, Antifungal properties of Schiff bases of chitosan, N-substituted chitosan and quaternized chitosan, Carbohydr. Res. 342 (2007) 1329–1332.
[25] M.J. O'Donnell, The enantioselective synthesis of α-amino acids by phase-transfer catalysis with achiral Schiff base esters, Acc. Chem. Res. 37 (2004) 506–517.
[26] P. Przybylski, A. Huczynski, K. Pyta, B. Brzezinski, F. Bartl, Biological properties of Schiff bases and azo derivatives of phenols, Curr. Org. Chem. 13 (2009) 124–148.
[27] N. Roy, H.A.R. Pramanik, P.C. Paul, T.S. Singh, A highly sensitive and selective fluorescent chemosensor for detection of Zn^{2+} based on a Schiff base, Spectrochim. Acta A. 140 (2015) 150–155.
[28] N. Roy, A. Dutta, P. Mondal, P.C. Paul, T.S. Singh, A new coumarin based dual functional chemosensor for colorimetric detection of Fe^{3+} and fluorescence turn-on response of Zn^{2+}, Sens. Actuators B Chem. 236 (2016) 719–731.
[29] D. Maity, A. Mukherjee, S.K. Mondal, P. Roy, Modulation of fluorescence sensing properties of quinoline-based chemosensor for Zn^{2+}: application in cell imaging studies, J. Lumin. 210 (2019) 508–518.
[30] M.S. Kim, S.Y. Lee, J.M. Jung, C. Kim, A new Schiff-base chemosensor for selective detection of Cu^{2+} and Co^{2+} and its copper complex for colorimetric sensing of S^{2-} in aqueous solution, Photochem. Photobiol. Sci. 16 (2017) 1677–1689.
[31] V.M. Herrera-Ambriz, J.L. Maldonado, M. Rodríguez, R. Castro-Beltrán, G. Ramos-Ortíz, N.E. Magaña-Vergara, M.A. Meneses-Nava, O. Barbosa-García, R. Santillan, N. Farfán, F.X. Dang, P.G. Lacroix, I. Ledoux-Rak, Highly efficient photorefractive organic polymers based on benzonitrile Schiff bases nonlinear chromophores, J. Phys. Chem. C 115 (2011) 23955–23963.
[32] J.R. Lakowicz, Principles of Fluorescence Spectroscopy, 3rd edn, Springer, New York, 2006.
[33] M.J. Frisch, G.W. Trucks, H.B. Schlegel, G.E. Scuseria, M.A. Robb, J.R. Cheeseman, G. Scalmani, V. Barone, B. Mennucci, G.A. Petersson, H. Nakatsuji, M. Caricato, X. Li, H.P. Hratchian, A.F. Izmaylov, J. Bloino, G. Zheng, J.L. Sonnenberg, M. Hada, M. Ehara, K. Toyota, R. Fukuda, J. Hasegawa, M. Ishida, T. Nakajima, Y. Honda, O. Kitao, H. Nakai, T. Vreven, J.J.A. Montgomery, J.E. Peralta, F. Ogliaro, M. Bearpark, J.J. Heyd, E. Brothers, K.N. Kudin, V.N. Staroverov, R. Kobayashi, J. Normand, K. Raghavachari, A. Rendell, J.C. Burant, S.S. Iyengar, J. Tomasi, M. Cossi, N. Rega, N.J. Millam, M. Klene, J.E. Knox, J.B. Cross, V. Bakken, C. Adamo, J. Jaramillo, R. Gomperts, R.E. Stratmann, O. Yazyev, A.J. Austin, R. Cammi, C. Pomelli, J.W. Ochterski, R.L. Martin, K. Morokuma, V.G. Zakrzewski, G.A. Voth, P. Salvador, J.J. Dannenberg, S. Dapprich, A.D. Daniels, O. Farkas, J.B. Foresman, J.V. Ortiz, J. Cioslowski, D.J. Fox, Gaussian 09, Revision A.02, Gaussian, Inc., Wallingford, CT, 2009.
[34] A.D. Becke, Density-functional thermochemistry. III. The role of exact exchange, J. Chem. Phys. 98 (1993) 5648–5652.
[35] C. Lee, W. Yang, R.G. Parr, Development of the Colic-Salvetti correlation-energy formula into a functional of the electron density, Phys. Rev. B 37 (1988) 785–789.
[36] T. Yanai, D.P. Tew, N.C. Handy, A new hybrid exchange–correlation functional using the coulomb attenuating method (CAM-B3LYP), Chem. Phys. Lett. 393 (2004) 51–57.
[37] T. Yanai, R.J. Harrison, N.C. Handy, Multiresolution quantum chemistry in multiwavelet bases: time-dependent density functional theory with asymptotically corrected potentials in local density and generalized gradient approximations, Mol. Phys. 103 (2005) 413–424.
[38] M.J.G. Peach, T. Helgaker, P. Sałek, T.W. Keal, O.B. Lutnæs, D.J. Tozer, N.C. Handy, Assessment of a coulomb-attenuated exchange–correlation energy functional, Phys. Chem. Chem. Phys. 8 (2006) 558–562.
[39] M. Cossi, N. Rega, G. Scalmani, V. Barone, Energies, structures, and electronic properties of molecules in solution with the CPCM solvation model, J. Comput. Chem. 24 (2003) 669–681.
[40] Y. Takano, K.N. Houk, Benchmarking the conductor-like polarizable continuum model (CPCM) for aqueous solvation free energies of neutral and ionic organic molecules, J. Chem. Theory Comput. 1 (2005) 70–77.
[41] O. Trott, A.J. Olson, Auto Dock Vina, Improving the speed and accuracy of docking with a new scoring function, efficient optimization, and multithreading, J. Comput. Chem. 31 (2010) 455–461.
[42] D. Seeliger, B.L. de Groot, Ligand docking and binding site analysis with PyMOL and Autodock/Vina, J. Comput. Aided Mol. Des. 24 (2010) 417–422.
[43] M.W. Chang, C. Ayeni, S. Breuer, B.E. Torbett, Virtual screening for HIV protease inhibitors: a comparison of AutoDock 4 and Vina, PLoS One 5 (2010) 1–9 e11955.
[44] R. Puliti, C.A. Mattia, L. Paduano, Crystal structure of a new α-cyclodextrin hydrate form. Molecular geometry and packing features: disordered solvent contribution, Carbohydr. Res. 310 (1998) 1–8.
[45] T. Aree, N. Chaichit, Crystal structure of β-cyclodextrin–dimethylsulfoxide inclusion complex, Carbohydr. Res. 337 (2002) 2487–2494.
[46] A. Nag, P. Chakraborty, G. Natarajan, A. Baksi, S.K. Mudedla, V. Subramanian, T. Pradeep, Bent keto form of curcumin, preferential stabilization of enol by piperine, and isomers of curcumin∩cyclodextrin complexes: insights from ion mobility mass spectrometry, Anal. Chem. 90 (2018) 8776–8784.
[47] http://www1.lsbu.ac.uk/water/cycloh.html.
[48] W.L. De Lano, The PyMOL Molecular Graphics System, De Lano Scientific, San Carlos, CA, 2004.
[49] A. Mallick, S. Maiti, B. Haldar, P. Purkayastha, N. Chattopadhyay, Photophysics of 3-acetyl-4-oxo-6,7-dihydro-12H indolo-[2,3-a] quinolizine: emission from two states, Chem. Phys. Lett. 371 (2003) 688–693.
[50] H.A. Benesi, J.H. Hildebrand, Spectrophotometric investigation of the interaction of iodine with aromatic hydrocarbons, J. Am. Chem. Soc. 71 (1949) 2703–2707.
[51] A. Chakrabarty, A. Mallick, B. Haldar, P. Das, N. Chattopadhyay, Binding interaction of a biological photosensitizer with serum albumins: a biophysical study, Biomacromolecules 8 (2007) 920–927.
[52] B.K. Paul, N. Guchhait, Exploring the strength, mode, dynamics, and kinetics of binding interaction of a cationic biological photosensitizer with DNA: implication on dissociation of the drug-DNA complex via detergent sequestration, J. Phys. Chem. B 115 (2011) 11938–11949.
[53] P. Das, A. Mallick, B. Haldar, A. Chakrabarty, N. Chattopadhyay, Effect of nanocavity confinement on the rotational relaxation dynamics: 3-acetyl-4-oxo-6,7-dihydro-12*H* indolo-[2,3-*a*] quinolizine in micelles, J. Chem. Phys. 125 (2006) 044516/1-6.
[54] P. Kundu, S. Ghosh, S. Das, N. Chattopadhyay, Cyclodextrin induced controlled delivery of a biological photosensitizer from a nanocarrier to DNA, Phys. Chem. Chem. Phys. 18 (2016) 3685–3693.
[55] S. Das, S. Ghosh, N. Chattopadhyay, Unprecedented high fluorescence anisotropy in protic solvents: Hydrogen bond induced solvent caging? Chem. Phys. Lett. 644 (2016) 284–287.
[56] A. Ray, S. Das, N. Chattopadhyay, Aggregation of nile red in water: its prevention through encapsulation in β-cyclodextrin, ACS Omega 4 (2019) 15–24.
[57] K.K. Rohatgi-Mukherjee, Fundamentals of Photochemistry, Wiley Eastern, New Delhi, 1992.
[58] A. Wu, X. Shen, Y. He, Investigation on γ-cyclodextrin nanotube induced by N,N′-diphenylbenzidine molecule, J. Colloid Interface Sci. 297 (2006) 525–533.
[59] S. Das, N. Chattopadhyay, Supramolecular inclusion-assisted disruption of probe-solvent network, ChemistrySelect 2 (2017) 6078–6081.